

Folding patterns in partially delaminated thin films

David Bourne, Sergio Conti and Stefan Müller

Abstract Michael Ortiz and Gustavo Gioia showed in the 90s that the complex patterns arising in compressed elastic films can be analyzed within the context of the calculus of variations. Their initial work focused on films partially debonded from the substrate, subject to isotropic compression arising from the difference in thermal expansion coefficients between film and substrate. In the following two decades different geometries have been studied, as for example anisotropic compression. We review recent mathematical progress in this area, focusing on the rich phase diagram of partially debonded films with a lateral boundary condition.

1 Introduction

Elastic films deposited on a substrate are often subject, after thermal expansion, to compressive strains which are released by debonding and buckling, generating a variety of microstructures. The work of Michael Ortiz and Gustavo Gioia in the 90s [1, 2] opened the way for the use of the tools of calculus of variations in the study of these structures. Their starting point was the Föppl-von Kármán plate theory, as given in (4) below. One of their insights was that the key nonconvexity which gives rise to the microstructure can be understood in terms of the out-of-plane displacement alone, leading after some rescalings to the Eikonal functional, as given in (1) below. This functional contains a term of the form $(|Dw|^2 - 1)^2$, where w is the normal displacement, which favours deformations with the property that the gradient of w is approximately a unit vector, independently of the orientation. Since

David Bourne
Department of Mathematical Sciences, Durham University

Sergio Conti
Institut für Angewandte Mathematik, Universität Bonn

Stefan Müller
Institut für Angewandte Mathematik, Universität Bonn

the film is still bound to the substrate at the boundary of the debonded region, the appropriate boundary condition is $w = 0$, which prescribes that the average over Ω of the gradient of w vanishes. Therefore the resulting low-energy deformations have gradient Dw oscillating between different values. As in many nonconvex variational problems, oscillations on very small scales may be energetically convenient, see [3, 4]. Correspondingly, the variational problem $\int_{\Omega} (|Dw|^2 - 1)^2 dx$ is not lower semicontinuous, and - depending on the boundary data and forcing - does not have minimizers. However, the curvature term $\sigma^2 |D^2 w|^2$ penalizes oscillations on an exceedingly fine scale and thereby ensures existence of minimizers. The solutions then have oscillations on an intermediate scale, which is determined by the competition between the two terms. The analysis of the specific functional proposed by Ortiz and Gioia is reviewed in Section 2 below.

The approach of Ortiz and Gioia was later extended to the full vectorial Föppl-von Kármán energy, and also to three-dimensional elasticity. These refinements explained the appearance of oscillations on two different length scales, with coarse oscillations in a direction normal to the boundary, and fine oscillations in the direction tangential to the boundary, as discussed in Section 3 below.

Recently interest has been directed to controlling the microstructures by designing the geometry of the debonded region appropriately [5, 6]. The key idea is to introduce a sacrificial layer between the film and the substrate, and then to selectively etch away a part of it, so that the boundary of the debonded region is straight. The film then partially rebonds to the surface, leading to complex patterns of tunnels. A study of these patterns within the Ortiz-Gioia framework, with a variational functional containing the Föppl-von Kármán energy and a fracture term proportional to the debonded area, is presented in Section 4. The mathematical analysis leading to the upper bounds of Theorem 6 suggests the presence of different types of patterns in different parameter ranges. The picture is rather easy in the two extreme cases in which the bonding energy per unit area is very small or very large. Indeed, in the first one the patterns observed for completely debonded films give the optimal energy scaling, in the second one the optimal state corresponds to the film completely bound to the substrate. In the intermediate regime we expect a richer picture, with bonded areas separated by thin debonded tunnels. For a certain regime, depending on the relation between the bonding energy per unit area, the film thickness and the compression ratio, a construction in which the tunnels branch and refine close to the boundary has a lower energy than the one with straight tunnels, see discussion in Section 4 below. The microstructure formation in thin films can be understood at a qualitative level as a form of Euler buckling instability. The relevant experiments, however, are well beyond the stability threshold, as discussed in Section 5 below.

2 Scalar modeling of compressed thin films

Ortiz and Gioia showed that, if tangential displacements are neglected, the energy of a compressed thin film can be characterized by the functional

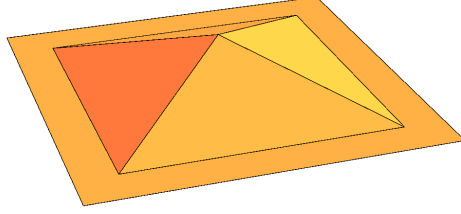


Fig. 1 Sketch of a deformation achieving the optimal energy in (1). Here the debonded region $\Omega = (0,1)^2$ is a square, and the distance to the boundary gives a “tent”-form. The convolution in (3) makes the folds then smooth transitions on a small scale.

$$I_\sigma[w] = \int_{\Omega} \left((|Dw|^2 - 1)^2 + \sigma^2 |D^2w|^2 \right) dx, \quad (1)$$

subject to $w = 0$ on $\partial\Omega$ and $w \geq 0$ in Ω . Here $\Omega \subset \mathbb{R}^2$ represents the debonded region, $w : \Omega \rightarrow [0, \infty)$ the rescaled normal displacement, and σ is a small parameter related to the thickness of the film. This functional arises also naturally in the study of liquid crystal configurations [7] and of magnetic structures in thin films [8]. Despite a large mathematical effort [7, 9, 10, 11, 12, 13, 14, 15] the problem (1) is not yet completely understood; it has been shown that the minimal energy is proportional to σ but the Γ -limit of $\sigma^{-1}I_\sigma[w]$ has only been partially identified. The natural candidate is

$$I_0[w] = \frac{1}{3} \int_{J_{Dw}} |[Dw]|^3 d\mathcal{H}^1 \quad (2)$$

restricted to functions $w : \Omega \rightarrow \mathbb{R}$ which solve the Eikonal equation $|Dw| = 1$ and are sufficiently regular. Here, J_{Dw} denotes the set of points (typically, a curve) where the gradient Dw is not continuous, $[Dw]$ denotes its jump across the interface, and $d\mathcal{H}^1$ the line integral along the interface. In particular, under the additional assumption that Dw is a function of bounded variation, it has been shown that for $\sigma \rightarrow 0$ the scaled functionals $\sigma^{-1}I_\sigma$ converge, in the sense of Γ -convergence, to I_0 , see [11, 12, 13] for the lower bound and [14, 15, 16] for the upper bound. However, it is also clear that finiteness of the energy does not imply that Dw has bounded variation, but only that w belongs to a larger space, called $AG(\Omega)$, see [11, 10]. Therefore the result is still incomplete.

The Eikonal equation $|Dw| = 1$ with the boundary data $w = 0$ on $\partial\Omega$ is solved by the distance to the boundary, $w_0(x) = \text{dist}(x, \partial\Omega)$. For example, if Ω is a square this leads to the tent-shaped deformation illustrated in Figure 1. The function w_0 is however only Lipschitz continuous, not twice differentiable, and makes the curvature term $\int_{\Omega} \sigma^2 |D^2w|^2 dx$ infinite. Therefore Ortiz and Gioia [1, 2] proposed to use a smoothed version of the distance function,

$$w_\sigma(x) = \int_{\Omega} \text{dist}(y, \partial\Omega) \varphi_\sigma(x-y) dy \quad (3)$$

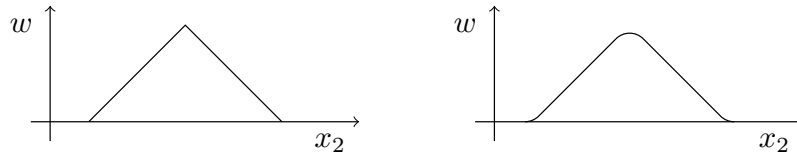


Fig. 2 Sketch of the effect of the mollification in (3) in a direction orthogonal to the fold. Left panel: the distance from the boundary $\text{dist}(x, \partial\Omega)$ is a function with slope ± 1 and sharp kinks. Right panel: the mollification defined in (3) still has slope ± 1 on large parts of the domain, but has smooth transitions from one value to the other over a length of the order of σ , see Figure 3.

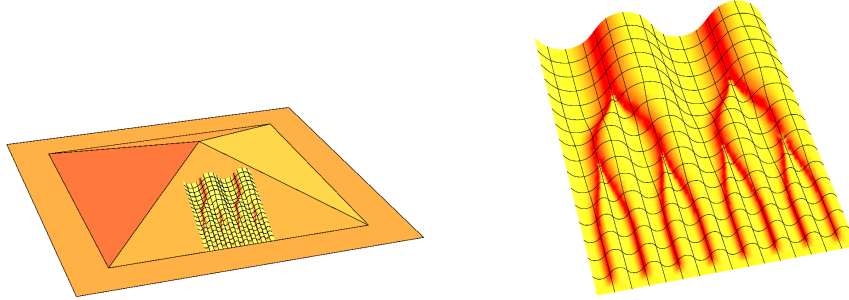


Fig. 3 Sketch of a deformation achieving the optimal upper bound in (5). As in Figure 1, the debonded region $\Omega = (0, 1)^2$ is a square. The starting point, at a coarse scale, is the “tent”-form illustrated in Figure 1. At a finer scale, folds orthogonal to the boundary relax the tangential compression (left panel, folds are only drawn in a small region). The period of the folds is of order h close to the boundary, and via a sequence of period-doubling steps becomes coarser in the inside (right, blow-up of the folds from the middle panel).

where φ_σ is a mollifier on the scale σ , i.e., $\varphi_\sigma \in C_c^\infty(B_\sigma)$ with $\int_{\mathbb{R}^2} \varphi_\sigma dx = 1$ and $|D\varphi_\sigma| \leq c/\sigma^3$. Then the regularized gradient Dw_σ has length close to 1 on most of the domain Ω , but at boundaries between regions where Dw_0 has different orientations Dw_σ changes smoothly over a length scale σ from one value to the other. The bending energy is correspondingly localized in a stripe of thickness 2σ around the interfaces, see Figure 2. The prediction that minimizers of (1) are well represented by w_σ is in good agreement, at least for some geometries, with experimental observations [1, 2].

The work of Ortiz and Gioia was then extended to related problems, showing for example that under anisotropic compression branching-type microstructures appear close to the boundary [17, 18], or that in certain regimes telephone-cord blisters develop [19, 20, 21] thanks to the interaction between the elastic deformation and the fracture problem that determines the boundary of the debonded region.

3 Pattern formation in debonded thin films

A finer analysis of the nonlinear elasticity model that had led to (1) showed that, in the case of isotropic compression, also the in-plane components exhibit fine-scale oscillations which refine close to the boundary [22, 23, 24, 25]. This analysis was based on the Föppl-von Kármán model, which includes the tangential components of the displacement u as well. After rescaling the energy takes the form (in the case of zero Poisson's ratio for simplicity)

$$E_\sigma[u, w] = \int_\Omega (|Du + Du^T + Dw \otimes Dw - \text{Id}|^2 + \sigma^2 |D^2 w|^2) dx. \quad (4)$$

Here $\Omega \subset \mathbb{R}^2$ is, as above, the debonded region, and the displacements u and w vanish at the boundary of Ω , corresponding to the fact that the rest of the film is still bound to the substrate. The isotropic compressive strain has been scaled to 1, and one can check that $E_\sigma[0, w] = 1 + I_\sigma[w]$. The key result from [22, 23] was that the minimum energy scales proportional to σ :

Theorem 1 (From [22, 23]). *Let $\Omega \subset \mathbb{R}^2$ be a bounded domain with piecewise smooth boundary. Then there are two constants $c_L, c_U > 0$ such that*

$$c_L \sigma \leq \min\{E_\sigma[u, w] : u = 0, w = 0 \text{ on } \partial\Omega\} \leq c_U \sigma. \quad (5)$$

The argument used for proving the lower bound also proves that a finite fraction of the energy is localized in a thin strip close to the boundary.

Similar statements hold if the plate theory in (4) is replaced by a fully three-dimensional nonlinear elastic model. For $v : \Omega \times (0, h) \rightarrow \mathbb{R}^3$, $h > 0$, we define

$$E_h^{3D}[v] = \frac{1}{h} \int_{\Omega \times (0, h)} W(Dv) dx \quad (6)$$

where $W : \mathbb{R}^{3 \times 3} \rightarrow [0, \infty)$ is the elastic stored energy density, which vanishes on the set of proper rotations $\text{SO}(3)$ and has quadratic growth, in the sense that

$$c \text{dist}^2(F, \text{SO}(3)) \leq W(F) \leq c' \text{dist}^2(F, \text{SO}(3)) \quad (7)$$

for some positive constants c and c' . The factor $1/h$ is included explicitly in (6) to obtain an energy per unit thickness, corresponding to (4).

In the nonlinear case the thickness h of the film and the compression δ enter the problem separately, however to leading order and after scaling the optimal energy only depends on the combination $\sigma = h/\delta^{1/2}$. In order to understand this expression it is instructive to recall the relation between the three-dimensional problem E_h^{3D} and its two-dimensional counterpart E_σ . In particular, a given pair (u, w) in (4) corresponds to a three-dimensional deformation v_δ of the form

$$v_\delta(x_1, x_2, x_3) = (1 - \delta) [\psi(x_1, x_2) + x_3 n(x_1, x_2)] \quad (8)$$

where

$$\psi(x_1, x_2) = \begin{pmatrix} x_1 + 2\delta u_1(x_1, x_2) \\ x_2 + 2\delta u_2(x_1, x_2) \\ (2\delta)^{1/2} w(x_1, x_2) \end{pmatrix} \quad (9)$$

represents the deformation of the $x_3 = 0$ layer and

$$n(x_1, x_2) = \begin{pmatrix} -(2\delta)^{1/2} \partial_1 w(x_1, x_2) \\ -(2\delta)^{1/2} \partial_2 w(x_1, x_2) \\ 1 \end{pmatrix} \quad (10)$$

is, to leading order, the normal to the surface described by ψ and gives the out-of-plane component of the strain. An expansion of $E_h^{3D}[v_\delta]$ for small δ shows that the leading order contribution is proportional to $\delta^2 E_\sigma[u, w]$ if the Poisson's ratio of the material vanishes. See for example [22, App. A and App. B] for a more detailed discussion of this point. A rigorous relation between E_σ and E_h^{3D} was derived in [26, 27] by means of Γ -convergence, these results however are appropriate for a different regime, with much smaller energy, and therefore do not apply directly to the situation of interest here.

Theorem 2 (From [25]). *Let $\Omega \subset \mathbb{R}^2$ be a bounded domain with piecewise smooth boundary, $\delta \in (0, 1)$, $h \in (0, \delta^{1/2})$. Then there are two constants $c_L, c_U > 0$ such that*

$$c_L \sigma \leq \min \left\{ \frac{1}{\delta^2} E_h^{3D}[u] : u(x) = (1 - \delta)x \text{ for } (x_1, x_2) \in \partial\Omega \right\} \leq c_U \sigma \quad (11)$$

where $\sigma = h/\delta^{1/2}$.

The significance of Theorem 1 and Theorem 2 is best understood by considering the key ideas in the proofs. The upper bound in (5) and (11) is proven by explicitly constructing a suitable deformation field (u, w) . This is done in several steps. The first step is the Ortiz-Gioia construction given in (3), which correctly describes the large-scale behavior of the film and relaxes the compression in direction normal to the boundary, as in Figure 1. In the second step one adds fine-scale oscillations in the orthogonal direction, as illustrated in Figure 3. This microstructure does not change the average shape significantly but relaxes the strain component tangential to the boundary. Finally, one realizes that optimal deformations have oscillations on a very fine scale close to the boundary, to adequately match the boundary data, but much coarser oscillations in the interior, to minimize the bending energy. Therefore a number of period-doubling steps are inserted, as illustrated in Figure 3. Analogous self-similar branched patterns had previously appeared in the study of microstructures in shape-memory alloys [28, 29], where for a simplified model it had been possible to show that minimizers are indeed asymptotically self-similar [30]. The scaling in the presence of finite elasticity, both of the martensite and in the surrounding austenite, was then studied in [31, 32]; vectorial variants of the model were considered in [33, 34]. A similar approach has been useful also for a variety of other problems, ranging from magnetic patterns in ferromagnets [35, 36, 37] to field

penetration in superconductors [38, 39], dislocation structures in crystal plasticity [40] and coarsening in thin film growth [41].

This variational approach to microstructure formation in thin elastic sheets is much more general, and indeed it can be applied to a number of related problems. One example is paper crumpling [42, 43] in which a thin plate, completely detached from the substrate, is confined to a small volume. In this case it has been possible to construct deformations with much smaller energy per unit volume. In particular one can obtain an energy per unit thickness proportional to $h^{5/3}$ [44, 45], and one can approximate any compressive deformation with this energy.

Theorem 3 (From [45]). *Let $\Omega \subset \mathbb{R}^2$ be a bounded domain, $r > 0$. Then there is a map $v : \Omega \times (0, h) \rightarrow B_r(0)$ such that*

$$E_h^{3D}[v] \leq ch^{5/3}. \quad (12)$$

The constant c may depend on Ω and r but not on h . Further, if $v_0 : \Omega \rightarrow \mathbb{R}^3$ is a short map, i.e., a map which obeys $|v_0(x) - v_0(y)| \leq |x - y|$ for all $x, y \in \Omega$, then there is a sequence v_h , converging to v_0 , such that

$$\lim_{h \rightarrow 0} \frac{1}{h^\alpha} E_h^{3D}[v_h] = 0 \quad (13)$$

for any $\alpha < 5/3$. Convergence of v_h is understood as uniform convergence of the vertical averages.

The proof of this is based on the combination of three ingredients. The first one is an approximation of short maps with origami maps:

Theorem 4 (From [45]). *Let $v_0 : \Omega \rightarrow \mathbb{R}^3$ be a short map, i.e., a map which obeys $|v_0(x) - v_0(y)| \leq |x - y|$ for all $x, y \in \Omega$. Then there is a sequence v_j of Origami maps converging uniformly to v_0 .*

Here we say that a map $v : \mathbb{R}^2 \rightarrow \mathbb{R}^3$ is an Origami map if it is continuous and piecewise isometric, i.e., if the domain can be subdivided into pieces such that v is a linear isometry (a translation plus a rotation) in each piece. The number of pieces is allowed to diverge only at infinity, in the sense that only finitely many pieces are allowed in any bounded subset of \mathbb{R}^2 .

The second step is to approximate any Origami maps with low-energy maps:

Theorem 5 (From [45]). *Let $\Omega \subset \mathbb{R}^2$ be a bounded domain, $v_0 : \Omega \times (0, h) \rightarrow B_r(0)$ be an Origami map. Then for any Origami map v_0 there is a sequence of maps $v_h : \Omega \times (0, h) \rightarrow \mathbb{R}^3$, converging to v_0 , such that*

$$E_h^{3D}[v_h] \leq Ch^{5/3}. \quad (14)$$

The constant may depend on Ω and v_0 but not on h .

This is proven by an explicit construction around each fold.

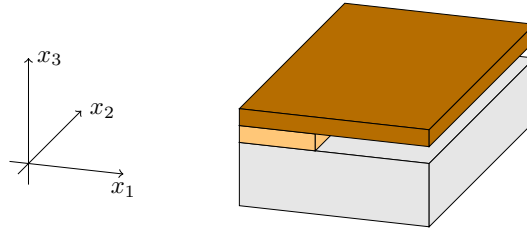


Fig. 4 Geometry of the partially delaminated film. The intermediate sacrificial layer is removed chemically only for $x_1 > 0$. The free-standing film is subject to compression at the Dirichlet boundary $x_1 = 0$ and may rebound to the substrate.

Another related problem of high current interest is the study of wrinkling patterns in graphene sheets [46, 47]. This has been addressed by a similar model, in which the boundary conditions are replaced by a viscous term describing the interaction with a substrate [48, 49, 50]. It would be interesting to see if the methods discussed here can be useful also for this variant of the problem.

4 Pattern formation in rebonded thin films

The microstructures spontaneously developed by compressed thin films can be controlled if the geometry of the debonded region is designed appropriately [5, 6]. One possibility is to introduce a sacrificial layer between the film and the substrate, and then to selectively etch away a part of it, so that the boundary of the debonded region is straight, see sketch in Figure 4. The film then partially rebonds to the surface, leading to complex patterns of tunnels, which in some cases refine close to the boundary, see Figure 5.

These patterns can be studied by coupling the von-Kármán energy with a fracture term proportional to the debonded area,

$$E_{\sigma, \gamma}[u, w] = \int_{\Omega} (|Du + Du^T + Dw \otimes Dw - \text{Id}|^2 + \sigma^2 |D^2 w|^2) dx + \gamma |\{w > 0\}|. \quad (15)$$

The three terms represent stretching, bending and bonding energies respectively. Here $u : \Omega \rightarrow \mathbb{R}^2$ are the (scaled) tangential displacements and $\gamma > 0$ is the bonding energy per unit area (related to Griffith's fracture energy), $|\{w > 0\}|$ represents the area of the set where the vertical displacement w is nonzero. Equivalently one could take the debonded state as reference and consider a negative term proportional to the rebonded area, $-\gamma |\{w = 0\}|$; the two energies only differ by an additive constant. The appropriate boundary conditions correspond to the film being bound to a substrate on one side of the domain; for simplicity we shall focus on $\Omega = (0, 1)^2$ with $u = 0$ and $w = 0$ on the $\{x_1 = 0\}$ side of Ω . As above, we assume $w \geq 0$ everywhere.

Fig. 5 Experimental picture of tube branching in $\text{Si}_{1-x}\text{Ge}_x$ film on a thick SiO_2 substrate. Experimental picture removed for copyright reasons, please see [5, Fig. 2].

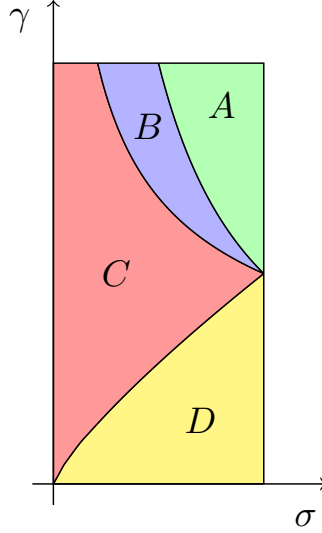


Fig. 6 Phase diagram for $E_{\sigma, \gamma}[u, w]$ in the (σ, γ) plane.

The mathematical analysis of the energy (15) leads to the rich phase diagram sketched in Figure 6, which contains four different regimes [51] that we now illustrate.

For large specific bonding energy γ the film is completely bound to the substrate. In particular the film is flat, so that there is no bending energy, but the stretching energy is not released. The total energy is then proportional to the area of Ω , and one obtains $E_{\sigma, \gamma}[0, 0] = 2$. This is regime A in Figure 6 and Theorem 6.

The opposite case of very small bonding energy γ is also easy to understand after the foregoing discussion: here the bonding term plays no significant role and the film is completely detached from the substrate. One recovers the result of the blistering problem of Theorem 1, $E_{\sigma, \gamma}[u, w] \simeq E_{\sigma}[u, w] \leq c\sigma$. The corresponding deformations are those illustrated in Figure 3. This is regime D in Figure 6 and Theorem 6.

For intermediate values of γ the situation is more complex, in particular debonded channels are formed, which separate wider bonded regions. In regime B the pattern is periodic and, away from the Dirichlet boundary, depends only on the tangential variable x_2 . A large part of the film is bonded to the substrate, but bonded regions are separated by thin tubes, see Figure 7. Denoting by h the period of the oscillations, and by δ the width of a tube, the total volume fraction of the tubes is δ/h , therefore the bonding energy is proportional to $\gamma\delta/h$. Each tube has to release a compression of h over a width δ , therefore the term $|Dw|^2$ is of order h/δ inside the tubes (the stretching energy is then completely relaxed). This gives $|Dw| \sim (h/\delta)^{1/2}$ in the tubes, and hence $|D^2w| \sim (h/\delta)^{1/2}/\delta$. Therefore the total energy can be estimated

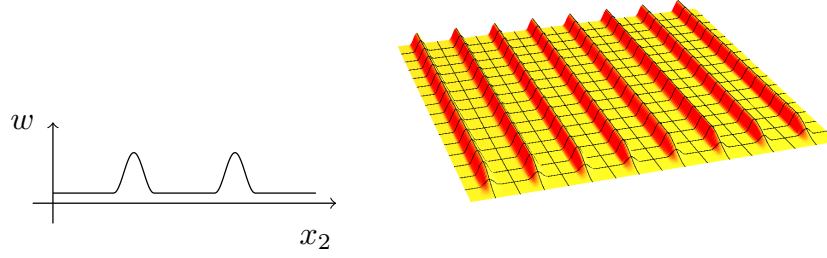


Fig. 7 Sketch of the laminate regime (B).

by

$$\gamma \frac{\delta}{h} + \sigma^2 \frac{\delta}{h} \left(\frac{h^{1/2}/\delta^{1/2}}{\delta} \right)^2 = \gamma \frac{\delta}{h} + \frac{\sigma^2}{\delta^2}. \quad (16)$$

Optimizing in δ we obtain $\delta \sim \sigma^{2/3} h^{1/3} \gamma^{-1/3}$ (this is clearly only admissible if $\delta \leq h \leq 1$). The period h is fixed by the energetic cost of the interpolation region close to the boundary. In this part of the domain there is no stretch-free construction, and indeed an interpolation over a boundary layer of thickness ε results in a total stretching energy of $\varepsilon(1 + h^2/\varepsilon^2)$. Optimizing over ε we obtain $\varepsilon \sim h$, and therefore the total energy for the laminate construction is

$$h + \gamma \frac{\delta}{h} + \frac{\sigma^2}{\delta^2}. \quad (17)$$

Inserting the value of δ obtained above and minimizing in h we conclude that h and E are proportional to $(\sigma\gamma)^{2/5}$. The width of each tube δ is then proportional to $\sigma^{4/5}\gamma^{-1/5}$. This is regime B in Figure 6; a precise version of this construction proves the second bound in Theorem 6.

If the bending term becomes more important, it is convenient to insert period-doubling steps, just like in the discussion of the functional (4). The resulting pattern is shown in Figure 8. In comparison to the pattern of Figure 3 the key difference is that the bending is localized to a small region, whereas large parts of the film are bond to the substrate. The period-doubling steps are only possible at the expense of stretching energy; balancing the different terms one finds [51] that the resulting energy is proportional to $\sigma^{1/2}\gamma^{5/8}$. The result of the construction is summarized in the following statement.

Theorem 6 (From [51]). *Let $\gamma > 0$, $\sigma \in (0, 1)$. There are u, w which obey the stated boundary conditions and*

$$E_{\sigma,\gamma}[u, w] \leq c \begin{cases} 1 & \text{if } \sigma\gamma > 1 & (\text{regime A}), \\ (\sigma\gamma)^{2/5} & \text{if } \sigma^{-4/9} \leq \gamma \leq \sigma^{-1} & (\text{regime B}), \\ \sigma^{1/2}\gamma^{5/8} & \text{if } \sigma^{4/5} \leq \gamma \leq \sigma^{-4/9} & (\text{regime C}), \\ \sigma & \text{if } \gamma < \sigma^{4/5} & (\text{regime D}). \end{cases} \quad (18)$$

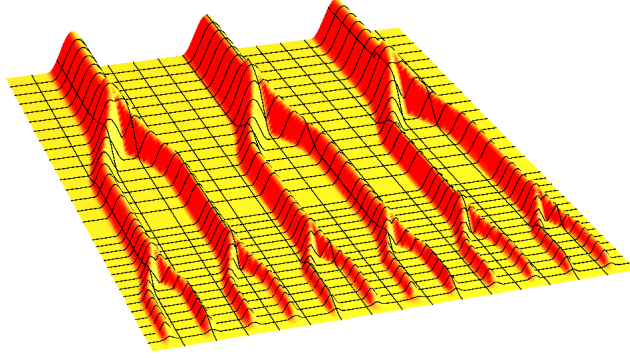


Fig. 8 Sketch of the tube branching regime (C).

The proof is based on making the constructions sketched above precise, details are given in [22] for regime D and in [51] for regimes B and C. Regime A, as discussed above, is immediate.

Optimality of the phase diagram just discussed can be at least partially proven by providing matching lower bounds on the energy. In particular, one can show the following.

Theorem 7 (From [51]). *Let $\gamma > 0$, $\sigma \in (0, 1)$. For any u, w which obey the stated boundary conditions one has*

$$E_{\gamma, \sigma}[u, w] \geq c \begin{cases} 1 & \text{if } \sigma\gamma > 1 & (\text{regime A}), \\ (\sigma\gamma)^{2/3} & \text{if } \sigma^{1/2} \leq \gamma \leq \sigma^{-1} & (\text{regime B'}), \\ \sigma & \text{if } \gamma < \sigma^{1/2} & (\text{regime D'}). \end{cases} \quad (19)$$

Whereas the statement in regime D' follows from [22], the other two bounds are proven in [51] using the Korn-Poincaré inequality for SBD^2 functions obtained in [52].

Theorem 7 proves optimality in phases A and D. The bound in the intermediate region does not, however, match the upper bounds stated in Theorem 6. Therefore it is at this stage not clear if the branching patterns illustrated in Figure 8 are optimal.

5 Linear stability analysis

The general form of the linearized Föppl-von Kármán plate theory under isotropic compression is [53, 54]

$$E_{\text{FVK}}[u, w] = \frac{1}{2} Yh \int_{\Omega} \left[(1 - \nu)|\varepsilon|^2 + \nu(\text{Tr}\varepsilon)^2 + \frac{h^2}{12} [(1 - \nu)|D^2w|^2 + \nu(\Delta w)^2] \right] dx, \quad (20)$$

see also [2, 22] for a discussion in the present context and [27] for a rigorous mathematical derivation. Here $\nu \in [-1, 1/2]$ is the Poisson ratio, Y Young's modulus, h the film thickness, and the strain ε is defined by

$$\varepsilon = Du + (Du)^T + Dw \otimes Dw - 2\delta \text{Id}, \quad (21)$$

where δ is the eigenstrain (i.e., the compression enforced by the substrate). We recall that we use $|M|^2 = \text{Tr}M^T M$ for the matrix norm. For $\nu = 0$, after a rescaling (20) reduces to (4). We recall that in [22, App. B] it was shown that the scaling behavior of the functional E_{FVK} is the same for all $\nu \in (-1, 1/2]$, hence our results hold also for generic values of the Poisson ratio. Of course, the regime $\nu \geq 0$ is the most relevant.

For small δ one can linearize around the state $u = 0, w = 0$. After straightforward computations this leads to

$$E_{\text{FVK}}^{\text{lin}}[u, w] = \frac{1}{2} Y h \int_{\Omega} \left[(1 - \nu) |Du + Du^T - 2\delta \text{Id}|^2 - 4\delta |Dw|^2 + \nu (2\text{div}u - 4\delta)^2 - 8\delta \nu |Dw|^2 + \frac{h^2}{12} [(1 - \nu) |D^2 w|^2 + \nu (\Delta w)^2] \right] dx.$$

In this linearized functional u and w are decoupled. The dependence on u is convex, hence $u = 0$ is the minimizer with the given boundary data. The dependence on w is however not necessarily convex. Working for concreteness in a circle of radius R , we can assume w to be radial, $w(x) = \varphi(|x|)$, subject to $\varphi(R) = 0$, so that

$$Dw(x) = \varphi'(|x|) \frac{x}{|x|}$$

and

$$D^2 w(x) = \varphi''(|x|) \frac{x}{|x|} \otimes \frac{x}{|x|} + \varphi'(|x|) \left(\frac{\text{Id}}{|x|} - \frac{x \otimes x}{|x|^3} \right).$$

Inserting into the energy leads to the one-dimensional variational problem

$$\frac{1}{2} Y h \int_0^R \left[-4\delta(1 + 2\nu)(\varphi'(r))^2 + \frac{h^2}{12} \left[(\varphi''(r))^2 + \left(\frac{\varphi'(r)}{r} \right)^2 + 2\nu \frac{\varphi'(r)\varphi''(r)}{r} \right] \right] r dr.$$

This is positive definite if the first term, of order δ , is not larger than the second term, of order h^2/R^2 . Therefore the loss of stability, which corresponds to Euler buckling, occurs at strains $\delta \sim h^2/R^2$. Inserting the experimental data from [5], namely, $h \sim 20$ nm, $R \sim 10$ μ m, $\nu \sim 0.277$, leads to $\delta_{\text{crit}} \sim 4 \cdot 10^{-6}$, which corresponds to a strain of 0.0004%. This is over three orders of magnitude smaller than the experimentally applied strain $\delta_{\text{Exp}} \sim 0.011 = 1.1\%$. Therefore the experiments we discussed take place well beyond the loss of linear stability, and a buckling-postbuckling analysis

does not seem appropriate to understand the deformations. Our variational approach is instead constructed to deal with deformations and microstructures that appear in the deeply nonlinear regime and is therefore more suitable to study the mentioned experiments.

Acknowledgements

This work was partially supported by the Deutsche Forschungsgemeinschaft through SFB 1060.

References

1. M. Ortiz, G. Gioia, *J. Mech. Phys. Solids* **42**, 531 (1994)
2. G. Gioia, M. Ortiz, *Adv. Appl. Mech.* **33**, 119 (1997)
3. B. Dacorogna, *Direct methods in the calculus of variations, Applied Mathematical Sciences*, vol. 78 (Springer-Verlag, Berlin, 1989)
4. S. Müller, in *Calculus of variations and geometric evolution problems*, ed. by F. Bethuel, et al. (Springer-Verlag, 1999), Springer Lecture Notes in Math. 1713, pp. 85–210
5. Y. Mei, D.J. Thurmer, F. Cavallo, S. Kiravittaya, O.G. Schmidt, *Advanced Materials* **19**, 21242128 (2007)
6. P. Cendula, S. Kiravittaya, Y.F. Mei, C. Deneke, O.G. Schmidt, *Phys. Rev. B* **79**, 085429 (2009)
7. P. Aviles, Y. Giga, *Proc. Centre Math. Anal. Austr. Nat. Univ.* **12**, 1 (1987)
8. A. DeSimone, R.V. Kohn, S. Müller, F. Otto, in *ICIAM 1999*, vol. 131 (Oxford University Press, 1999), vol. 131, pp. 833–844
9. P. Aviles, Y. Giga, *Proc. Roy. Soc. Edin. Sect. A* **126**, 923 (1996)
10. P. Aviles, Y. Giga, *Proc. Roy. Soc. Edin. A* **129**, 1 (1999)
11. L. Ambrosio, C. De Lellis, C. Mantegazza, *Calc. Var. Partial Diff. Eqs.* **9**, 327 (1999)
12. W. Jin, R.V. Kohn, *J. Nonlinear Sci.* **10**, 355 (2000)
13. A. DeSimone, R.V. Kohn, S. Müller, F. Otto, *Proc. Roy. Soc. Edin. A* **131**, 833 (2001)
14. A. Poliakovsky, *J. Eur. Math. Soc. (JEMS)* **9**(1), 1 (2007)
15. S. Conti, C.D. Lellis, *Math. Ann.* **338**, 119 (2007)
16. A. Poliakovsky, *C. R. Math. Acad. Sci. Paris* **341**, 97 (2005)
17. G. Gioia, A. DeSimone, M. Ortiz, A.M. Cuitino, *Proc. Roy. Soc. London Ser. A* **458**, 1223 (2002)
18. S. Conti, A. DeSimone, S. Müller, *Comp. Meth. Appl. Mech. Eng.* **194**, 2534 (2005)
19. G. Gioia, M. Ortiz, *Acta Mater.* **46**(1), 169 (1998)
20. B. Audoly, *Phys. Rev. Lett.* **83**, 4124 (1999)
21. B. Audoly, *J. Mech. Phys. Solids* **48**, 2315 (2000)
22. H. Ben Belgacem, S. Conti, A. DeSimone, S. Müller, *J. Nonlinear Sci.* **10**, 661 (2000)
23. W. Jin, P. Sternberg, *J. Math. Phys.* **42**, 192 (2001)
24. W. Jin, P. Sternberg, *Proc. R. Soc. Edin. A* **132A**, 911 (2002)
25. H. Ben Belgacem, S. Conti, A. DeSimone, S. Müller, *Arch. Rat. Mech. Anal.* **164**, 1 (2002)
26. G. Friesecke, R.D. James, S. Müller, *Comm. Pure Appl. Math.* **55**(11), 1461 (2002)
27. G. Friesecke, R.D. James, S. Müller, *Archive for Rational Mechanics and Analysis* **180**, 183 (2006)
28. R.V. Kohn, S. Müller, *Phil. Mag. A* **66**, 697 (1992)

29. R.V. Kohn, S. Müller, *Comm. Pure Appl. Math.* **47**, 405 (1994)
30. S. Conti, *Comm. Pure Appl. Math.* **53**, 1448 (2000)
31. S. Conti, *Cont. Mech. Thermod.* **17**, 469 (2006)
32. B. Zwicknagl, *Arch. Ration. Mech. Anal.* **213**, 355 (2014)
33. J. Diermeier, Master's thesis, Universität Bonn (2013)
34. A. Chan, S. Conti, *Math. Models. Methods App. Sci.* **25**, 1091 (2015)
35. R. Choksi, R.V. Kohn, *Comm. Pure Appl. Math.* **51**, 259 (1998)
36. R. Choksi, R.V. Kohn, F. Otto, *Comm. Math. Phys.* **201**, 61 (1999)
37. T. Viehmann, Uniaxial ferromagnets. Ph.D. thesis, Universität Bonn (2009)
38. R. Choksi, R.V. Kohn, F. Otto, *Journal of Nonlinear Science* **14**, 119 (2004)
39. R. Choksi, S. Conti, R.V. Kohn, F. Otto, *Comm. Pure Appl. Math.* **61**, 595 (2008)
40. S. Conti, M. Ortiz, *Arch. Rat. Mech. Anal.* **176**, 103 (2005)
41. S. Conti, M. Ortiz, *J. Mech. Phys. Solids* **56**, 1885 (2008)
42. A.E. Lobkovsky, S. Gentges, H. Li, D. Morse, T.A. Witten, *Science* **270**, 1482 (1995)
43. T.A. Witten, *Rev. Mod. Phys.* **79**, 643 (2007)
44. S.C. Venkataramani, *Nonlinearity* **17**, 301 (2004)
45. S. Conti, F. Maggi, *Arch. Rat. Mech. Anal.* **187**, 1 (2008)
46. X. Li, W. Cai, J. An, S. Kim, et al., *Science* **324**, 1312 (2009)
47. J. Zang, S. Ryu, N. Pugno, Q. Wang, Q. Tu, M.J. Buehler, X. Zhao, *Nature Materials* **12**, 321325 (2013)
48. K. Zhang, M. Arroyo, *J. Appl. Phys.* **113**, 193501 (2013)
49. K. Zhang, M. Arroyo, *J. Mech. Phys. Solids* **72**, 61 (2014)
50. M. Arroyo, K. Zhang, M. Rahimi, IUTAM Symposium on innovative numerical approaches for materials and structures in multi-field and multi-scale problems (2014)
51. D. Bourne, S. Conti, S. Müller, In preparation (2015)
52. A. Chambolle, S. Conti, G. Francfort, Preprint hal-01091710v1 (2014)
53. S.S. Antman, *Nonlinear Problems in elasticity*. No. 107 in Applied Math. Sciences (Springer-Verlag, 1995)
54. P.G. Ciarlet, *Theory of plates, Mathematical elasticity*, vol. II (Elsevier, Amsterdam, 1997)